# FUEL ASSEMBLY SHAKER AND TRUCK TEST SIMULATION

## Fuel Cycle Research & Development

*Prepared for*
*U.S. Department of Energy*
*Used Fuel Disposition Campaign*
*Nicholas Klymyshyn*
*Philip Jensen*
*Scott Sanborn*
*Brady Hanson*

*Pacific Northwest National Laboratory*
*September 30, 2014*

*FCRD-UFD-2014-000328*
*PNNL-23688*

**Reviewed by:**

Project Manager

| | |
|---|---|
| Signature on file | 9/30/2014 |
| Brady Hanson | Date |

# SUMMARY

This report fulfills the requirement of milestone M3FT-14PN0813034 “Shaker Table Report” under work package FT-14PN081303.

This study continues the modeling support of the Sandia National Laboratories (SNL) shaker table task from 2013 and includes analysis of the SNL 2014 truck test campaign. Detailed finite element models of the fuel assembly surrogate used by SNL during testing form the basis of the modeling effort. Additional analysis was performed to characterize and filter the accelerometer data collected during the SNL testing.

The detailed fuel assembly finite element model was modified to improve the performance and accuracy of the original surrogate fuel assembly model in an attempt to achieve a closer agreement with the low strains measured during testing. The revised model was used to recalculate the shaker table load response from the 2013 test campaign. As it happened, the results remained comparable to the values calculated with the original fuel assembly model. From this it is concluded that the original model was suitable for the task and the improvements to the model were not able to bring the calculated strain values down to the extremely low level recorded during testing. The model needs more precision to calculate strains that are so close to zero.

The truck test load case had an even lower magnitude than the shaker table case. Strain gage data from the test was compared directly to locations on the model. Truck test strains were lower than the shaker table case, but the model achieved a better relative agreement of 100-200 microstrains (or 0.0001-0.0002 mm/mm).

The truck test data included a number of accelerometers at various locations on the truck bed, surrogate basket, and surrogate fuel assembly. This set of accelerometers allowed an evaluation of the dynamics of the conveyance system used in testing. It was discovered that the dynamic load transference through the conveyance has a strong frequency-range dependency. This finding suggests that different conveyance configurations could behave differently and transmit different magnitudes of loads to the fuel even when traveling down the same road at the same speed. It is recommended that the SNL conveyance system used in testing be characterized through modal analysis and frequency response analysis to provide context and assist in the interpretation of the strain data that was collected during the truck test campaign.

# CONTENTS

# FIGURES

## TABLES

# ACRONYMS

| | |
|---|---|
| DFT | discreet Fourier transform |
| EI | beam bending stiffness |
| FEA | finite element analysis |
| NCT | Normal Conditions of Transport |
| PNNL | Pacific Northwest National Laboratory |
| SDOF | single degree of freedom |
| SNL | Sandia National Laboratories |
| SRS | shock response spectrum |
| UNF | used nuclear fuel |

# FUEL ASSEMBLY SHAKER AND TRUCK TEST SIMULATION

## 1. INTRODUCTION

This work is a continuation of analytical work started in 2012 and supports experimental shock and vibration testing performed by Sandia National Laboratories (SNL) on a surrogate used fuel assembly. A shaker table test campaign was conducted in 2013, and Pacific Northwest National Laboratory (PNNL) models of the fuel assembly were used in pre-test and post-test predictions of the fuel assembly behavior to the applied loads. The shaker table loads were selected to represent the shock and vibration environment that used fuel is expected to experience during highway transport. In 2014, the SNL test campaign used a tractor-trailer to simulate the over-the-road shock and vibration environment.

PNNL's modeling tasks for 2014 included updating the fuel assembly model, recalculating the 2013 shaker test model results, and performing post-test analysis of the SNL over-the-road testing. The reason for updating the fuel assembly model is to see if it brings the model even closer to agreement with the recorded cladding strain gage data. The post-test analysis of the over-the-road testing offers a chance to validate the PNNL fuel assembly model against experimental data. While analyzing the recorded test data, PNNL discovered an interesting physical phenomenon regarding the load transference through the test conveyance system that is documented in this report.

# 2. SHAKER TABLE MODEL UPDATE

A number of enhancements were made to the shaker table model fuel assembly. These enhancements were first applied to the fuel assembly model used in the *Normal Conditions of Transport (NCT) Modeling and Simulation Initial Demonstration* (Adkins et al. 2013), which used the 2013 version of the shaker table fuel assembly model as its starting basis. A number of the changes developed in the course of the NCT task are applicable for incorporation into the shaker table fuel assembly surrogate and enhance the physical accuracy or the computational efficiency of the model. This section describes the changes made to the shaker table model since the previous shaker table model effort (Klymyshyn et al. 2013).

The updates made to the shaker table model include:

- inclusion of gravity load
- simplification of upper and lower nozzle geometries
- reduction in the number of elements used in the grid meshes
- elimination of small guide tube elements
- modification of generalized weld connection between the guide tubes and the grids
- use of non-linear springs and dimples and changes to the dimple location.

Figure 2-1 shows the updated shaker model and the old shaker model. The supporting basket and other shaker table structures are identical; only the assembly has been modified.

An investigation was also made to determine if the bending stiffness of the lead filled copper rods should be increased to account for the stiffness of the lead. However, it was found that the beam bending stiffness (EI) (modulus of elasticity E multiplied by cross sectional area moment of inertia I) of the lead was essentially negligible compared to the EI of the copper. Therefore, no adjustment to the copper rod stiffness was made.

## 2.1 Inclusion of Gravity Load

The first modification made was to include the effects of gravity. The inclusion of gravity is thought to have a minor effect on the response of the shaker assembly. Nonetheless, it is more accurate to include gravity. Gravity was added by performing a separate analysis with gravity as the only load. There the global damping was increased until all dynamic effects were negligible. A preload file was generated and added to the full analysis.

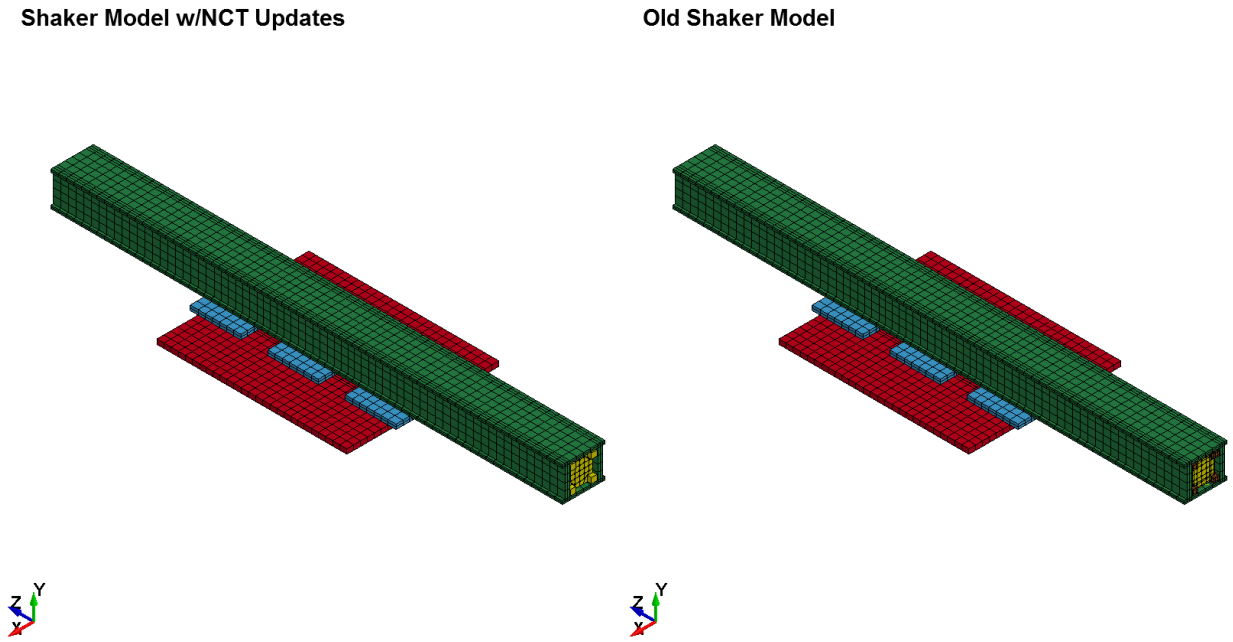


Figure 2-1: Overview of the entire shaker model with NCT updates (left) and the entire old shaker model (right).

## 2.2 Simplification of Upper and Lower Nozzle Geometries

The top and bottom nozzle geometries were simplified to improve the mesh and the minimum time step at the cost of geometry accuracy, which was not particularly important for the shaker table analysis.

Figure 2-2 shows the comparison between the updated shaker table top nozzle and the old shaker table top nozzle. The old top nozzle was split into three parts for the plate, the side walls, and the rim. The updated top nozzle is just one part with only one material property assigned. The updated nozzle has a slightly thicker plate and sidewall. The density of the updated top nozzle material was adjusted so that the top nozzle's mass remained the same.

Figure 2-3 shows the comparison between the updated shaker table bottom nozzle and the old shaker table bottom nozzle. The old bottom nozzle was also split into three parts for the plate, the legs, and the feet. The updated bottom nozzle is just one part with only one material property assigned. The updated bottom nozzle has simpler leg/foot geometry. The density of the updated bottom nozzle material was adjusted so that the bottom nozzle's mass remained the same.

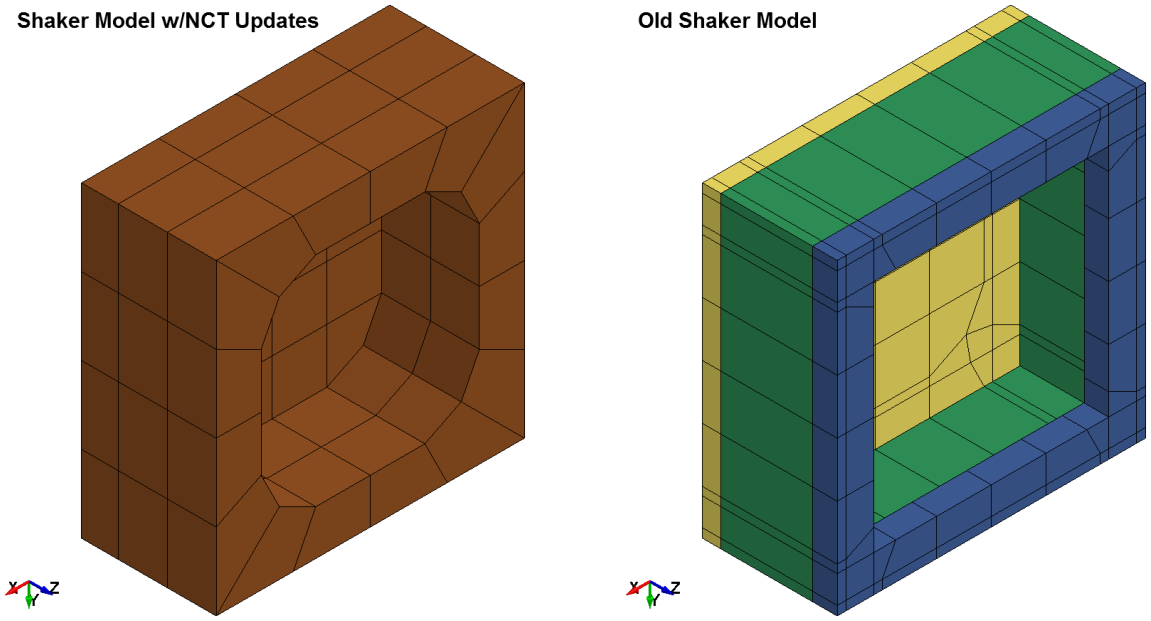


Figure 2-2: Top end nozzle geometries for the updated shaker table model (left) and the old shaker table model (right).

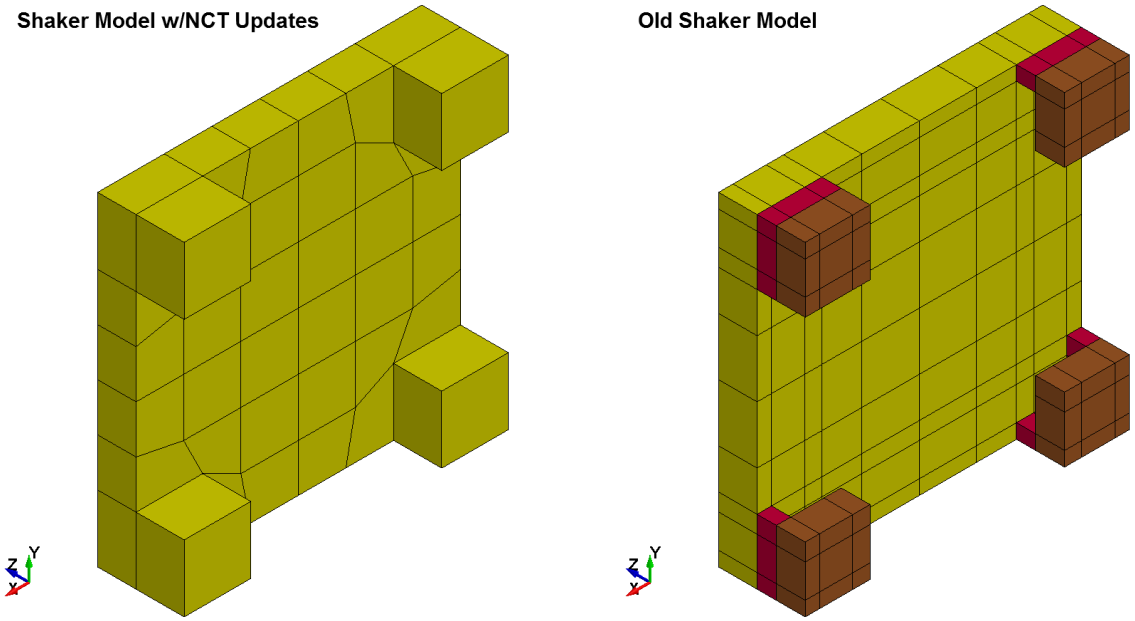


Figure 2-3: Bottom end nozzle geometries for the updated shaker table model (left) and the old shaker table model (right).

## 2.3 Reduction in the Number of Elements Used in the Grid Meshes

To increase the minimum time step, the number of elements used in the grids was reduced. Figure 2-4 shows the comparison between grid meshes on the bottom two grids for the updated shaker table model and the old shaker table model. For each grid slot, the number of shell elements per slot has been reduced from sixteen (old model) to eight (updated model). Like the

old shaker table model, the updated shaker table model takes advantage of the tied-nodes-to-surface contact to connect the springs and dimples to the grids without the need for a specific node in the location where the spring or dimple meets the grid.

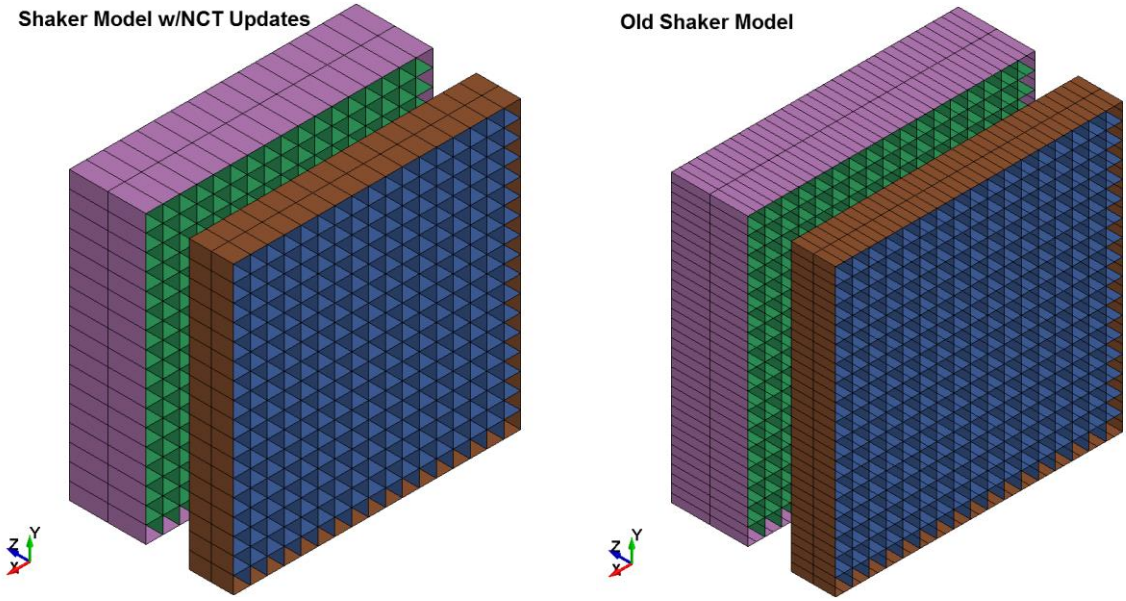


Figure 2-4: The meshes used in the grids are shown for the updated shaker table model (left) and the old shaker table model (right).

## 2.4 Elimination of Small Guide Tube Elements

The guide tube elements were modified. A number of short or small guide tube elements were eliminated. These small elements can be locations of unrealistic stress concentrations. Figure 2-5 shows a location where small guide tube elements were eliminated near the bottom of the assembly.

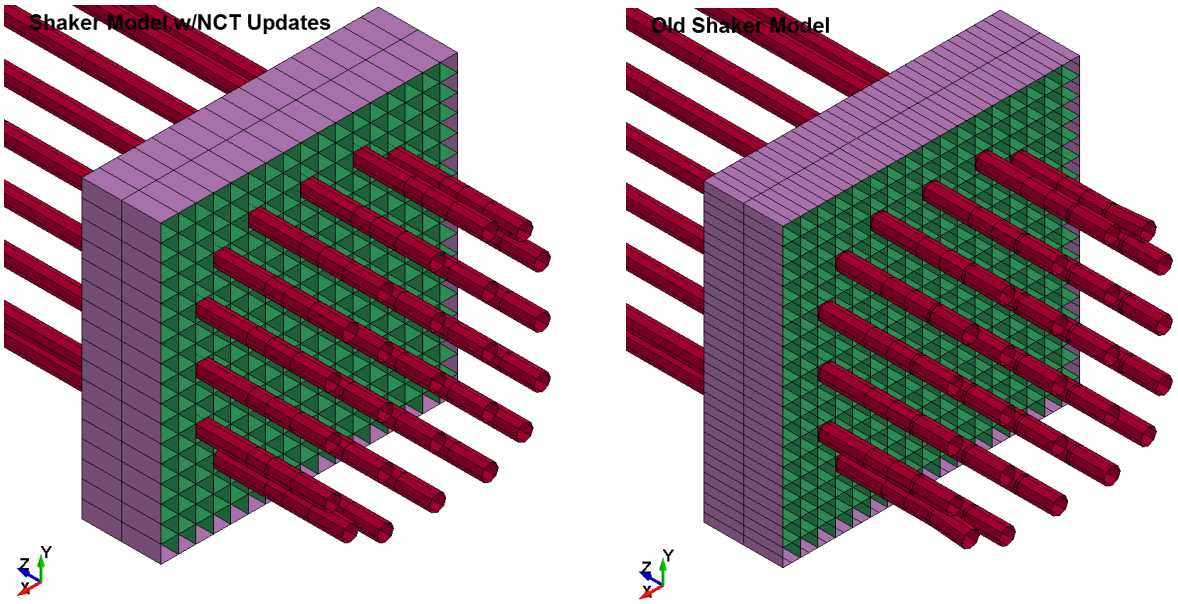


Figure 2-5: Guide tube elements near the bottom of the assembly in the updated shaker table model (left) and the old shaker table model (right).

## 2.5 Modification of Generalized Weld Connection Between the Guide Tubes and the Grids

The generalized weld connections between the guide tubes and the grids were modified. This modification results from the remeshing of the grids. With fewer elements per grid slot, there is no longer a node in the center of the slot to tie the guide tubes to. Instead, the weld connections use nodes in the corner of the slots. Figure 2-6 shows a cross-section of a grid with the generalized weld connections used in the updated shaker table model and the old shaker table model. Figure 2-7 shows a close-up view of these connections for one guide tube through one grid slot. Also apparent from this figure is that the outer weld connections are not all in one plane; the guide tube node has moved in slightly from the grid slot's edge. This movement is a result of the new dimple location discussed in the next section.

In addition to the change in geometry, the weld breaking force was set to an extremely high value, essentially making the welds unbreakable. The old shaker table model had a normal and tangential breaking force set to 3.7E5 N; however, under previous shaker table analysis, these welds never experienced breakage. Because the guide-tube-to-grid connection is essentially a swage rather than a weld, the very high breaking force is more appropriate as the connection would then always fail by plastic strain in the guide tubes or grids.

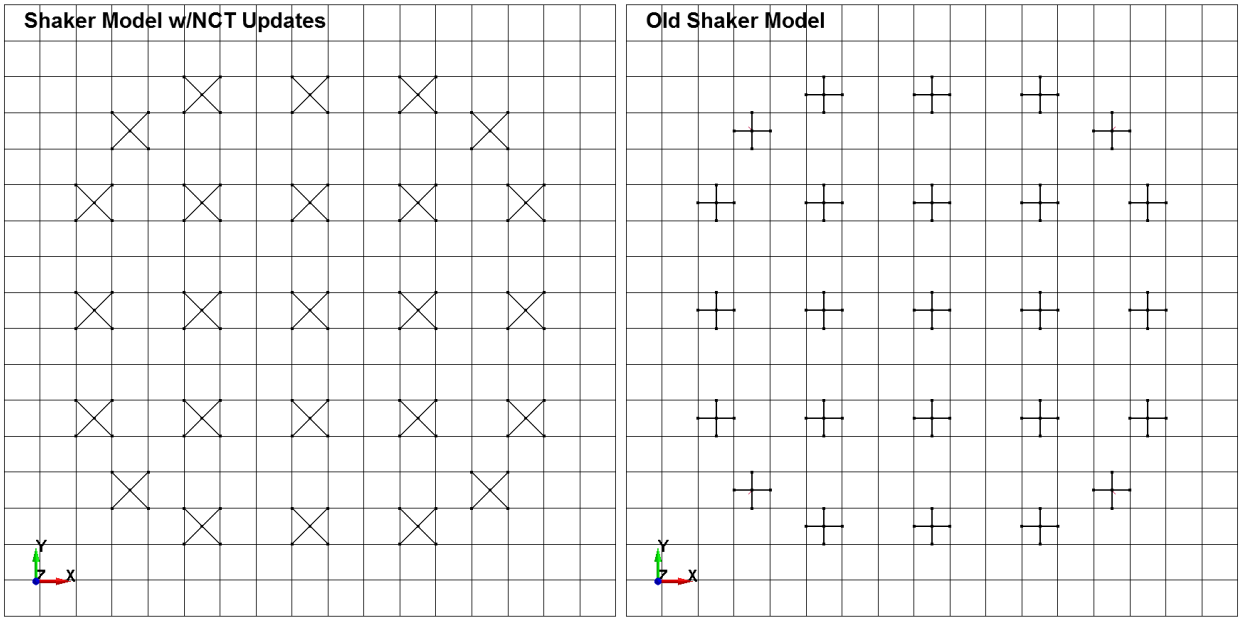


Figure 2-6: Cross-section of a grid showing the generalized weld connections in the updated shaker table model (left) and the old shaker table model (right).

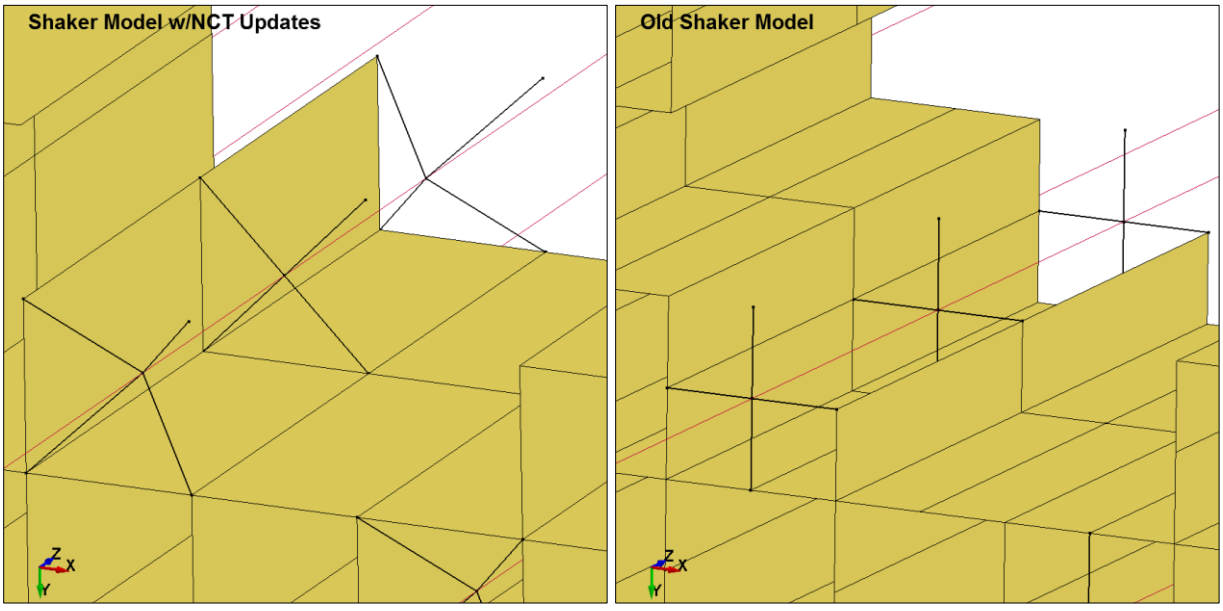


Figure 2-7: Close-up of one guide tube and the generalized weld connection through one grid in the updated shaker table model (left) and the old shaker table model (right). Note: Grid beam elements are represented as red lines, and several grid elements have been made invisible for this figure.

## 2.6 Use of Non-linear Springs and Dimples and Changes to the Dimple Location

In the old shaker model, the copper rods were connected to the grids using linear springs with no distinction between springs and dimples. In the NCT Initial Demonstration (Adkins et al. 2013), studies were performed to determine the appropriate connection between the fuel rods and the grids. Single grid slot models were used to determine non-linear force-displacement curves for both the springs and the dimples. The studies performed in the NCT Initial Demonstration were for material properties associated with Zircaloy and Inconel grids and the associated high burnup fuel. While this situation differs from the shaker table setup, in the absence of a more detailed study of the shaker table assembly grid slots, the Zircaloy force-displacement curves from the NCT Initial Demonstration are adopted in the updated shaker table model. Figure 2-8 shows the force-displacement curves used in the updated shaker table model for the springs and dimples. Both curves have a zero force for a zero displacement, meaning there is no preload on these springs or dimples. The stiffness for both the spring and dimple is greater under compression compared to the spring or dimple under tension. The dimple is stiffer than the spring in compression but follows the same behavior in tension.

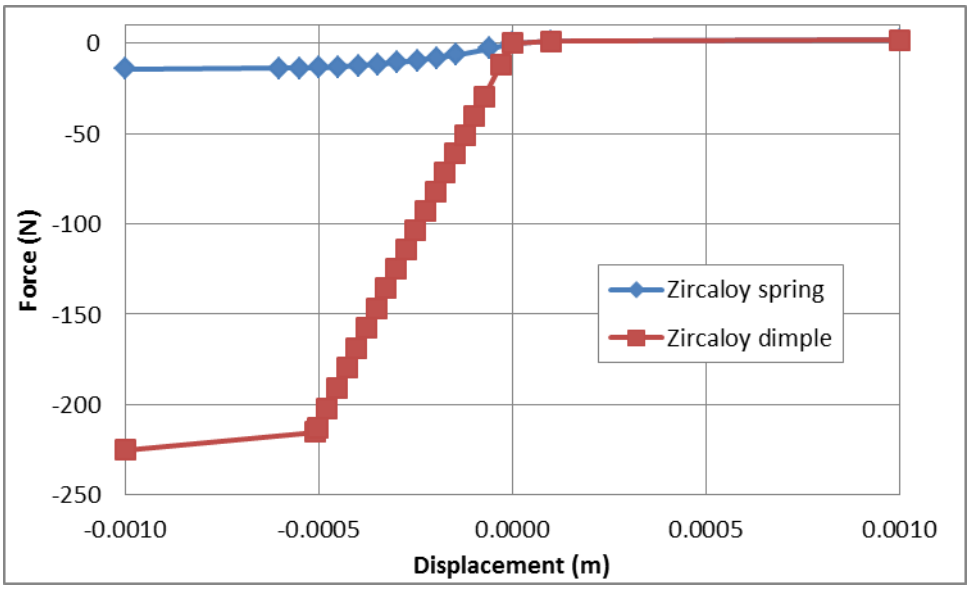


Figure 2-8: Force-displacement curves for the springs and dimples in the updated shaker table model.

Finally, as discussed above, the dimple's location was also moved from the old shaker table model to the updated shaker table model. In the old shaker table model, the dimples were assigned to act exactly on the spacer grid edge. However, during the NCT Initial Demonstration, review of several spacer grid designs showed an offset of the dimple location. The assembly model in the NCT Initial Demonstration offset this dimple location to act a distance of 10% of the total grid width from the edge of the grid. This 10% offset was also adopted here. The copper rods have nodes at this 10% difference, but as discussed above, the spacer grid elements do not. The dimples are attached to the spacer grid shell elements via the tie-nodes-to-surface contact definition at this 10% offset location.

## 2.7 Results

The load case evaluated with the revised model corresponds to the post-test evaluation documented in Section 4.3 of the 2013 PNNL report (Klymyshyn et al. 2013). The vertical acceleration load history is identified as Shock Realization #2 in the 2013 SNL shaker table test campaign. The acceleration time history was applied as a vertical nodal acceleration at the bottom of the anchor plate, which is the wide red plate beneath the fuel basket pictured in Figure 2-1. This load history shakes the fuel basket, transmitting loads to the detailed fuel assembly.

This report frequently discusses low-magnitude strains. The symbol με is used to denote a microstrain, where 1 με equals 0.000001 mm/mm.

The finite element analysis used the single-precision solver, which was determined in the 2013 report to offer a degree of accuracy that is sufficient for typical applications of the detailed fuel assembly model. The double-precision solver offers higher precision at the added cost of file size and computer run time. The 2013 study compared a similar detailed fuel assembly model subjected to shaker loads and found the average difference in calculated strain at each point in time was ±10 με, with a maximum instantaneous error of ±480 με. Considering the magnitude of strains expected here, the precision is something to consider when reviewing the results.

The finite element analysis (FEA) results are calculated to compare against experimental data collected by SNL. The same model is used in both the shaker test load case and highway test load case. The highway test configuration included four strain gage locations, designated as S1, S2, S3, and S4. These locations also correspond to strain gage locations used in the shaker test campaign. For consistency, the results of these four locations are reported for both sets of analysis. The shaker testing contained more strain gage locations, but the highest strains occurred in the S1-S4 locations.

The finite element model discretizes the cladding with a number of elements along its length. The strain gages are much smaller than the element size, so the available locations of calculated results do not line up precisely with strain gage locations. S1 and S3 are both located within the boundaries of elements, so the element peak stress and strain are reported. S2 and S4 are located at the middle of the span between spacer grids, which happens to be located between two elements. In these cases, the element with the greater strain is considered to be the representative element for S2 and S4. Table 2-1 identifies the elements of the cladding in Span 10 and Span 5.

Table 2-1: Strain gage mapping to FEA model.

| Gage | Element #s | Comments |
|---|---|---|
| - | - | Span 10 |
| S1 | 51558 | |
| S2 | 51559-51560 | Between two elements |
| S3 | 51561 | |
| - | - | Span 5 |
| S4 | 51548-51549 | Between two elements |

The peak strains calculated by the FEA model are reported in Table 2-2. The loading comes from shock realization #2, which had a peak absolute value of 213 μs. The latest version of the 2013 PNNL model calculated a peak strain value of 762 μs throughout the cladding, with strains at strain gage locations reported for comparison in Table 2-2. Model results were calculated out to a time of 2.27 seconds, which is expected to include the maximum strain value achieved during the test. As the table of results shows, the peak strain is 744 μs, which is approximately equal to the peak strain calculated by the 2013 version of the model. These results demonstrate that the model changes described in Section 2.0 do not significantly change the model behavior or improve its agreement with the reported very low strains.

Table 2-2: Shaker test calculated values.

| **Strain Gage** | **Peak FEA Strain (μs) Current (2014)** | **Peak FEA Strain (μs) Previous (2013)** |
|---|---|---|
| S1 - 0° | 626 | 465 |
| S2 - 0° | 744 | 578 |
| S3 - 0° | 635 | 376 |
| S4 - 0° | 589 | 496 |

# 3. HIGHWAY SHOCK ANALYSIS AND MODEL VALIDATION

The updated fuel assembly model described in Section 2.0 was loaded with a one-second window of acceleration data from the truck test. This particular time window was selected because it includes local peak strains for many of the cladding strain gages and is discussed in more detail in Section 4.1. This acceleration load was applied in a manner identical to the shaker simulation described in Section 2.7. The only change is the composition of the acceleration history, which is plotted in Figure 3-1. With a filtered peak acceleration of just 0.5 g, it was suspected that the road test load would be substantially weaker than the shaker table load, resulting in even lower strains than those predicted in Section 2.7. The relative strengths of the two mechanical shock load cases were evaluated before generating the finite element analysis results.

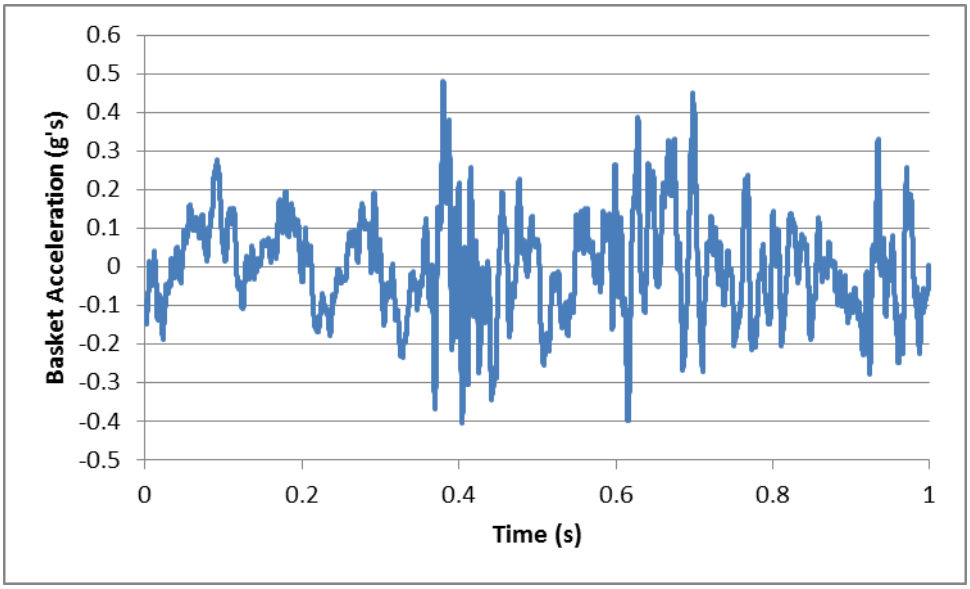


Figure 3-1: Basket acceleration applied as base excitation.

The comparison of shock load strengths was done by calculating a shock response spectrum (SRS) for each acceleration load history. SRS plots are a way of characterizing mechanical shock loads according to the response they generate from single degree of freedom (SDOF) spring/mass/damper systems. This comparison illustrates the fact that dynamic loads can have a stronger or weaker effect on a dynamic system depending on that system's natural frequency. (See Section 4.2 for a description of the SRS methodology used in this report.)

The results of the SRS evaluation are plotted in Figure 3-2. The plot shows that the shaker table excitation was relatively stronger for frequencies between 1 Hz and about 25 Hz. Between 3 Hz and 20 Hz, the difference is particularly significant, due to the difference in magnitude. The modal analysis documented in the 2013 shaker report shows that most of the strongest fuel assembly vibration modes are at 20 Hz and lower. The SRS evaluation suggests that a weaker dynamic response is expected for the truck load data.

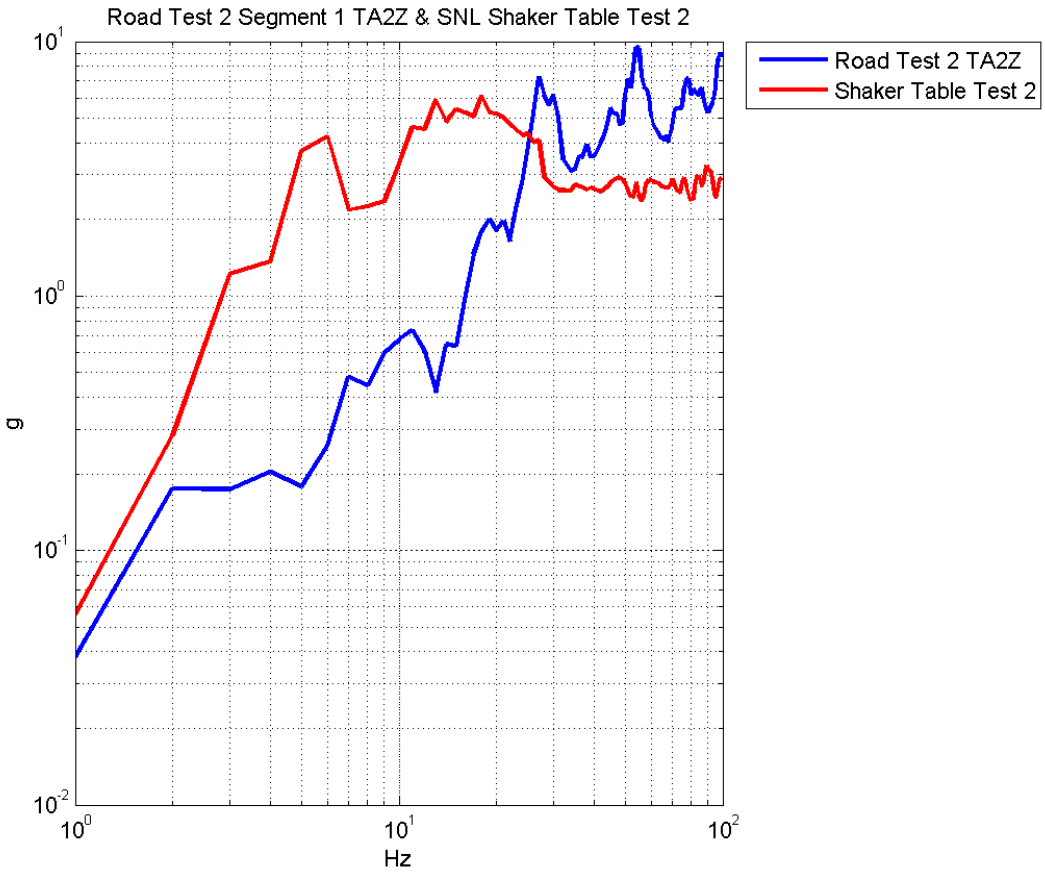


Figure 3-2: Comparative shock response spectra of model excitation.

The finite element analysis used the single precision solver. As discussed in Section 2.7, the accuracy of this model is expected to be on the order of ±10 µs on average, with the accuracy bounds of any particular point to be ±480 µs. Considering the magnitude of strains expected here, the precision is something to consider when reviewing the results.

The peak strains at each strain gage location are reported in Table 3-1. The peak FEA strain is the maximum integration point axial strain in µs. The peak recorded strain comes from the 0° location strain gage data recorded over the specific time window chosen for this analysis. In both cases, the absolute value is reported. All of the FEA peaks at the strain gage locations happened to be positive, while all of the strain gage data peaks happened to be negative.

Table 3-1: Highway load case FEA model results.

| Strain Gage | Peak FEA Strain (µs) | Peak Recorded Strain (µs) |
|---|---|---|
| S1 - 0° | 244 | 114 |
| S2 - 0° | 274 | 116 |
| S3 - 0° | 323 | 126 |
| S4 - 0° | 192 | 139 |

Figure 3-3 shows a direct comparison in the time domain of the calculated strain response compared to the strain gage data recorded during testing. The results appear to be a case where the FEA model does not have the precision necessary to calculate such small strains. Comparing the strain curves at each point in time, the FEA can be orders of magnitude in error, indicating that the model would require more refinement to be able to predict the strains below 100 µs. The use of the LS-DYNA double-precision solver is expected to reduce the error to a point, but the loads are so low that efforts to validate or improve the model with this experimental data set are not of practical value. A better loading regime for model validation would be closer to the yield limit of the zirconium alloy of the cladding (6,800 µs). With peak recorded strains near 100 µs, this would correspond to a two order of magnitude increase in loads.

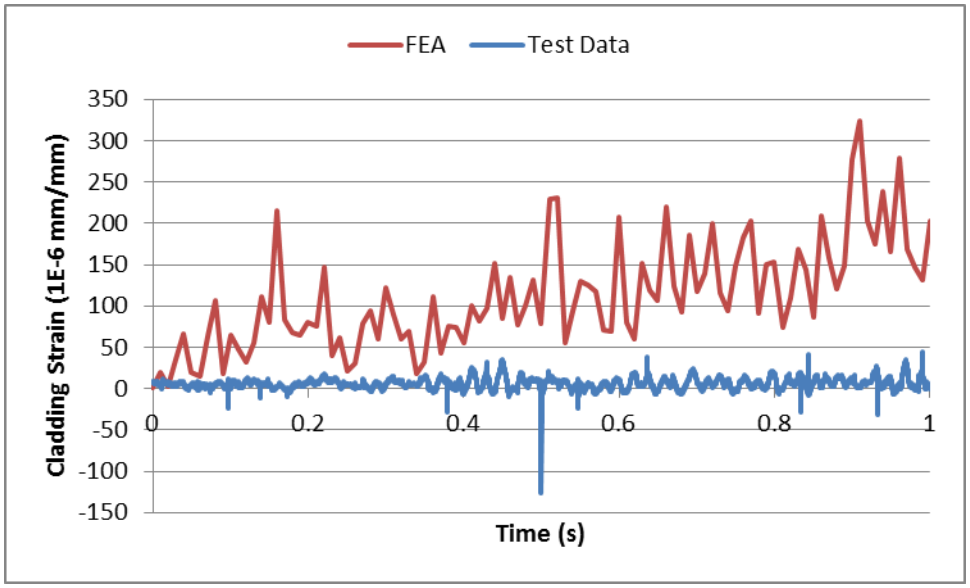


Figure 3-3: Direct comparison of strain history data.

# 4. HIGHWAY TEST DATA PROCESSING AND ANALYSIS

The highway tests performed by SNL provide valuable information regarding the loads transmitted through the conveyance system to the fuel assembly. For practical reasons, the testing could not be performed on an actual used nuclear fuel (UNF) conveyance system, so a surrogate test conveyance system was configured using a flatbed trailer and large blocks of concrete to achieve a realistic mass. PNNL used the accelerometer data to construct the load history described in Section 3.0.

The raw accelerometer data was filtered according to the methods described in Section 4.1. PNNL used a band-pass filtering scheme that eliminates low- and high-frequency content from the accelerometer signal. The high-end frequencies are expected to have no effect on the system response, and the low-end frequencies contain some phenomena that appear to be noise and signal drift. Their elimination permits a plausible construction of velocity and displacement histories that fit within the expected range of rigid body motion witnessed in testing.

The filtered accelerometer data is analyzed in Section 4.2 using a frequency range analysis to generate comparative SRS curves for all the accelerometers over a particular window of time. This analysis offers a comparison of the strength of the shock loading on a frequency-by-frequency basis. The data is evaluated over the range of 1 Hz to 99 Hz, at whole frequency intervals. The comparisons show that certain frequencies are transmitted more strongly through the system than others.

## 4.1 PNNL Filtering

SNL has performed a number of tests that measured the strains and accelerations relevant to the transport of used nuclear fuel during normal truck transport. For these tests, accelerometers were placed on the transport trailer, simulated basket, and mock-up fuel assembly. This section of the report describes the data analysis, which was done to determine a suitable load case for the analysis described in Section 4.0 and to understand the transference of dynamic loads from the road through the conveyance system.

The test data provided to PNNL consisted of the acceleration time histories measured in g's (the acceleration of gravity, 9.8 $m/s^2$). These time histories were filtered by applying a band pass filter generated in Matlab from 1Hz to 500 Hz. Information below 1 Hz was removed to discard low-frequency signal noise that affected the numerical integration of the accelerometer data and prevented the numerical integration of the accelerometer data. The numerical integration of the accelerometer data was necessary to obtain the velocity and displacement information. Information above 500 Hz was removed because previous work has indicated that frequencies above 500 Hz are not a major contributor to the excitation of fuel assemblies during transport.

To demonstrate the filter, Figure 4-1 below shows the unfiltered log-log plot of the discreet Fourier transform (DFT) for the Ch. 13 101Z assembly accelerometer, from the first segment of road test 1. Figure 4-2 shows the log-log plot of the DFT for the same accelerometer with the filter applied.

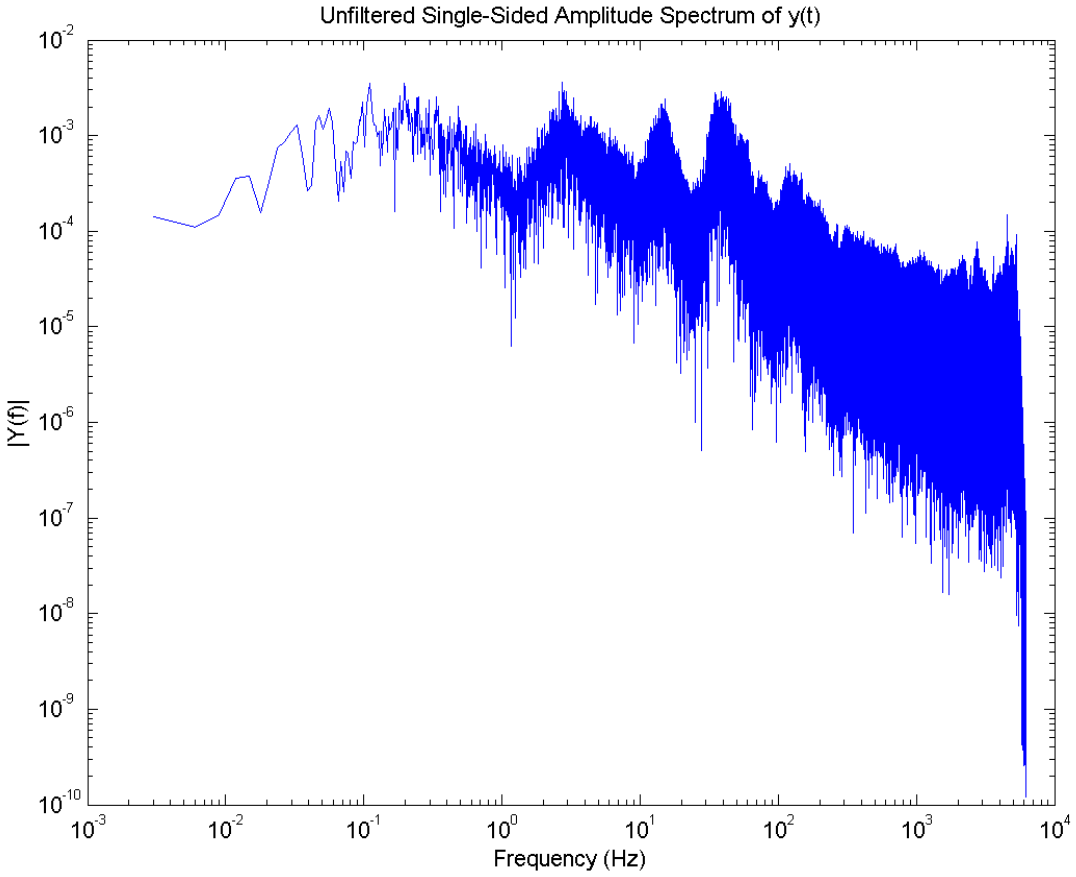


Figure 4-1: Unfiltered log-log plot of the DFT of ch. 13 101Z from segment 1 of road test 1.

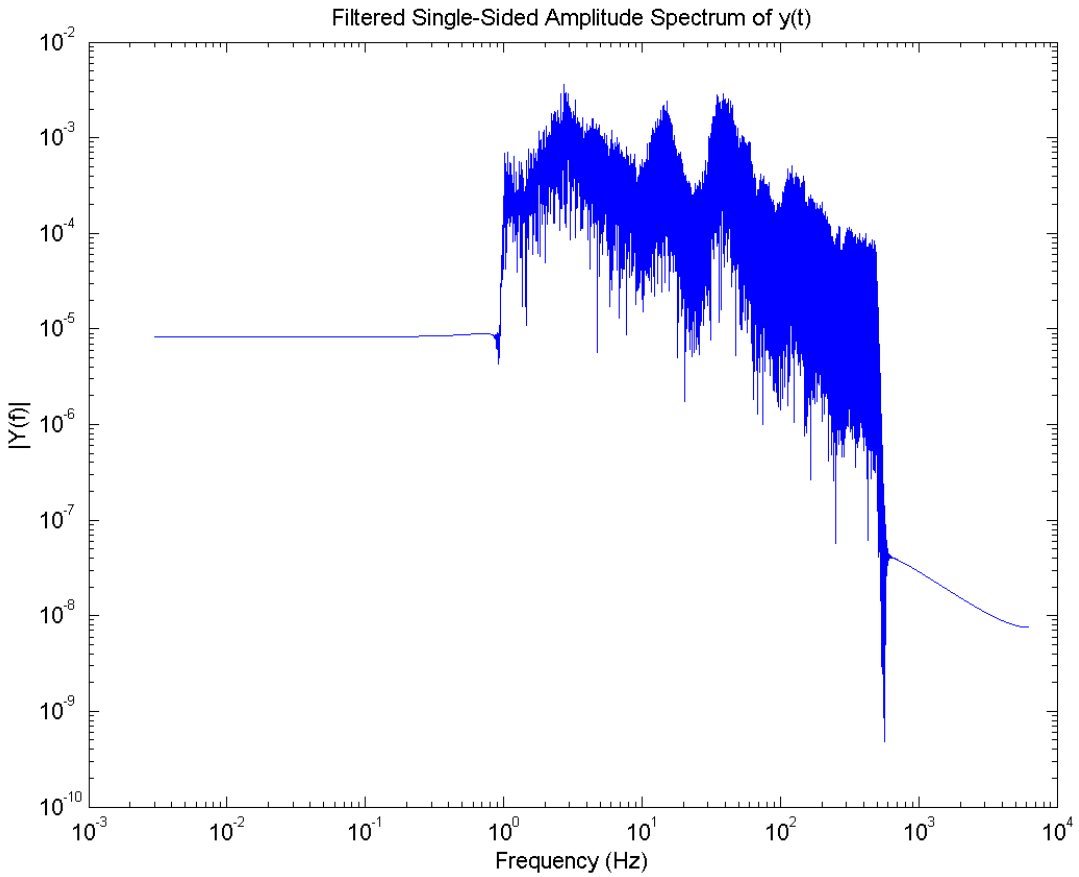


Figure 4-2: Filtered log-log plot of the DFT of ch. 13 101Z from segment 1 of road test 1.

As mentioned above, once the filter was applied, the acceleration data was numerically integrated to obtain the velocity and displacement. Figure 4-3 shows the filtered acceleration for the Ch. 13 101Z assembly accelerometer from the first segment of road test 1; Figure 4-4 shows the velocity for this accelerometer; and Figure 4-5 shows the displacement for this accelerometer. This accelerometer was located on the fuel assembly spacer grid nearest the top, so its data represents the motion of the top end of the fuel assembly.

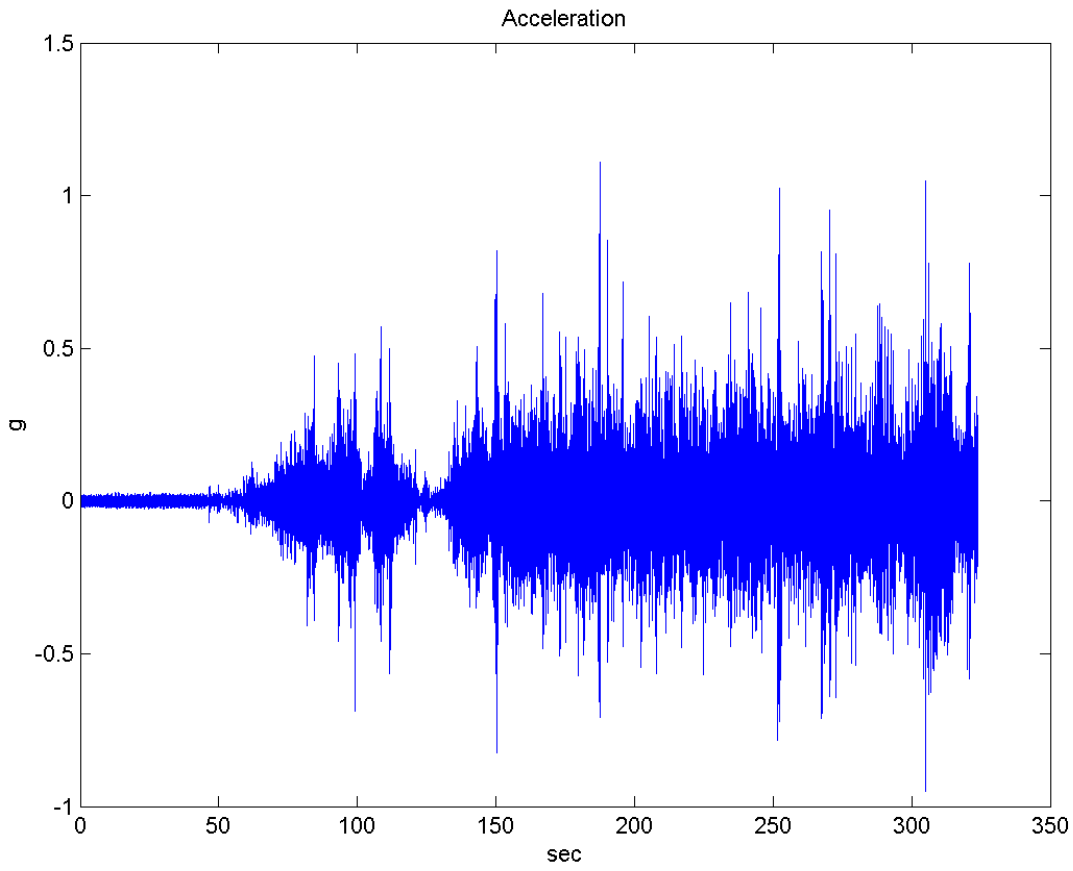


Figure 4-3: Filtered acceleration of ch. 13 101Z from segment 1 of road test 1.

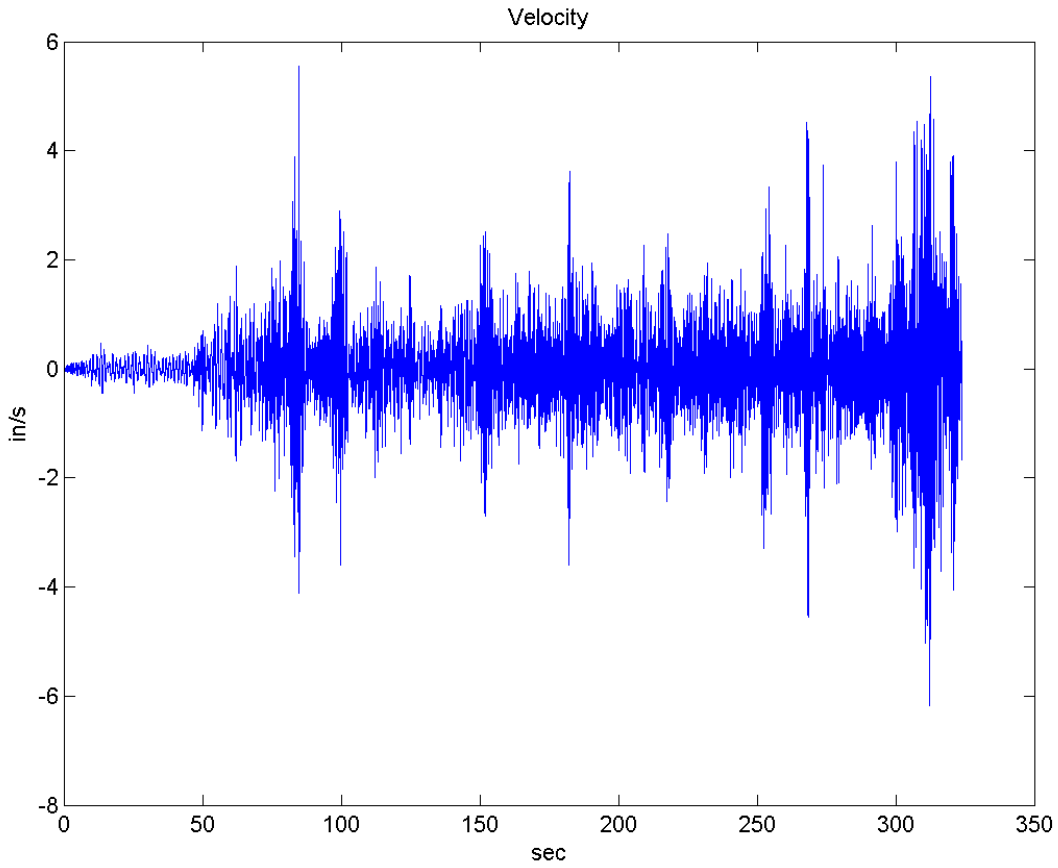


Figure 4-4: Velocity of ch. 13 101Z from segment 1 of road test 1.

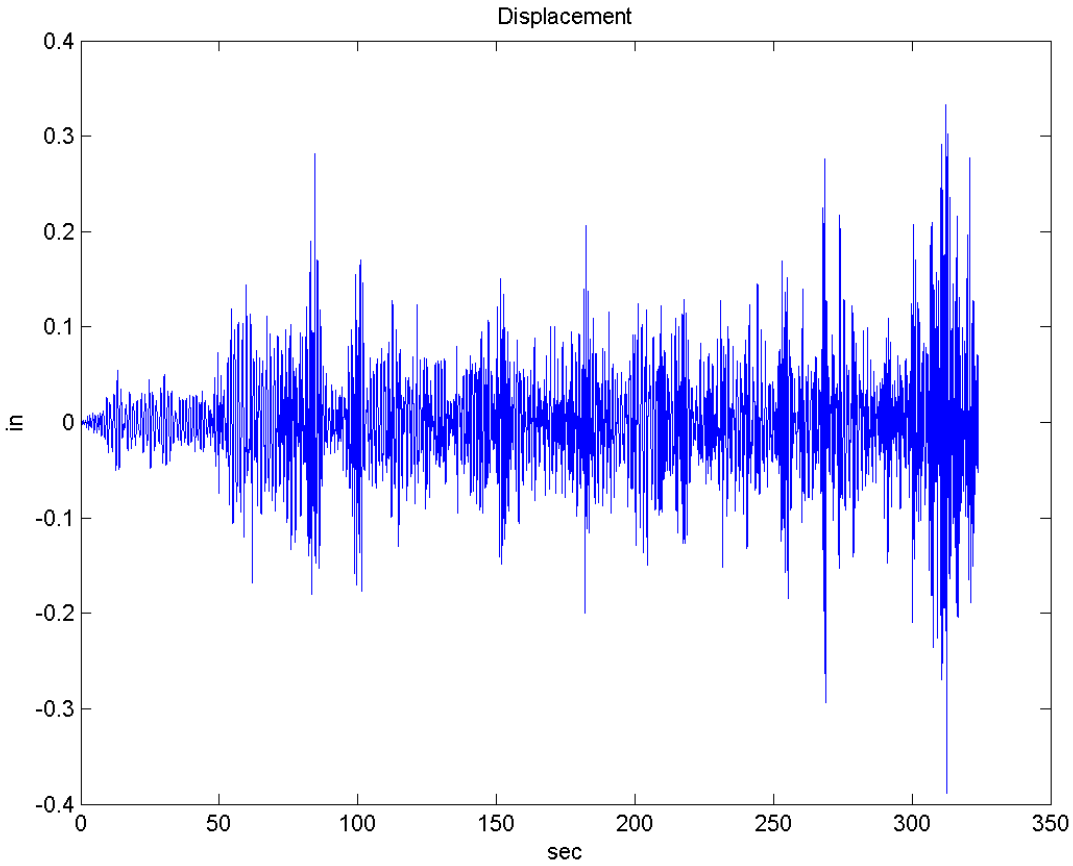


Figure 4-5: Displacement of ch. 13 101Z from segment 1 of road test 1.

From the filtered acceleration data, the maximum shock (i.e., the peak magnitude of acceleration) for that data set was identified, and a ten -second window around this shock was determined. The maximum shock for the Ch. 13 101Z assembly accelerometer from the first segment of road test 1 and the ten -second window around it are shown in Figure 4-6. This maximum shock window was used for comparison across the various accelerometers used in test program, with the results discussed in Section 4.2. This ten -second window is centered on 187.5 seconds into the first segment of road test 1.

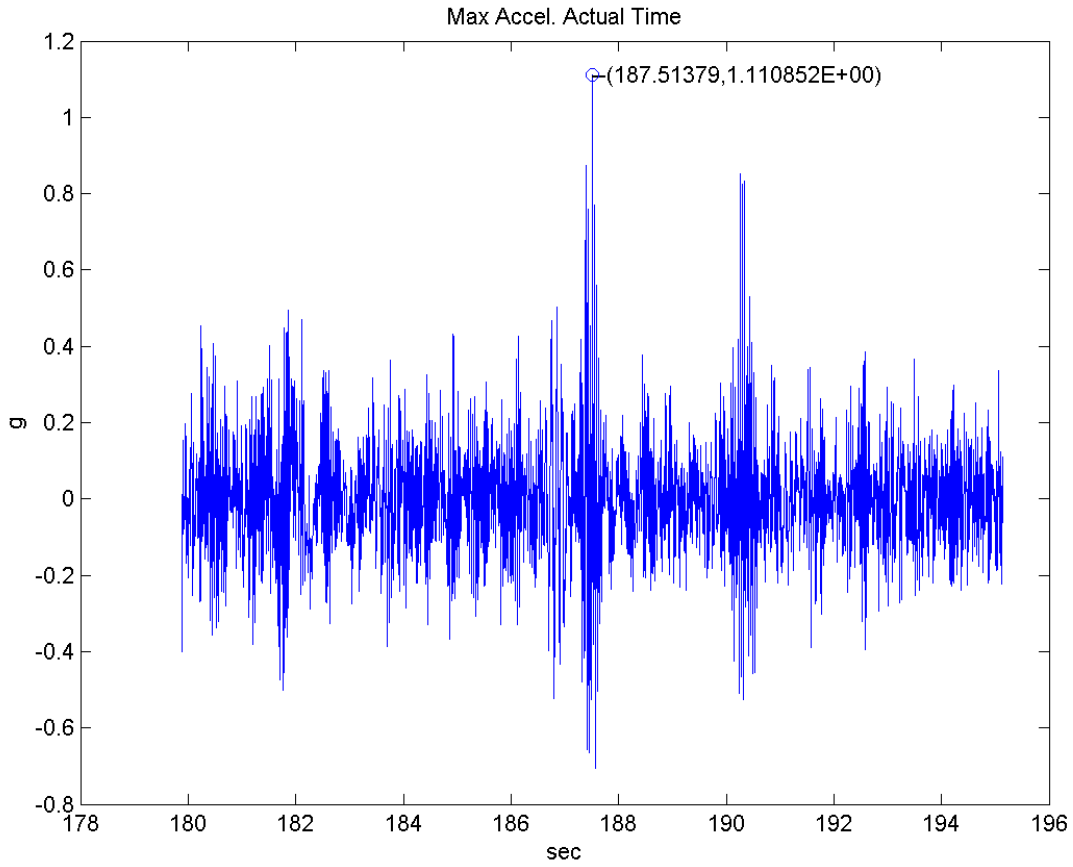


Figure 4-6: Max shock of ch. 13 101Z from segment 1 of road test 1.

A different shock window was chosen to represent the loading of the highway model and followed a different procedure. The key difference is that the highway load shock window was chosen based on peaks in the cladding strain gage data. Another difference is that the duration of the window was narrowed to one second due to the computation time required of the detailed fuel assembly model described in Section 2.0. The segment of time was taken from Segment 1 of the second road test series. Figure 4-7 shows the strain data from the S1, 0-degree strain gage. This window includes localized strain peaks of approximately 125 µs. The one-second window was centered on 789 seconds, which is roughly two minutes before the absolute peak reported by SNL in their report, which occurred at 896 seconds. The difference is that SNL was looking at the maximum strain at any one location, while PNNL attempted to capture multiple peaks in the same one-second window. Given the differences in filtering frequencies, the peak strains are very similar in magnitude and represent the maximum strain behavior.

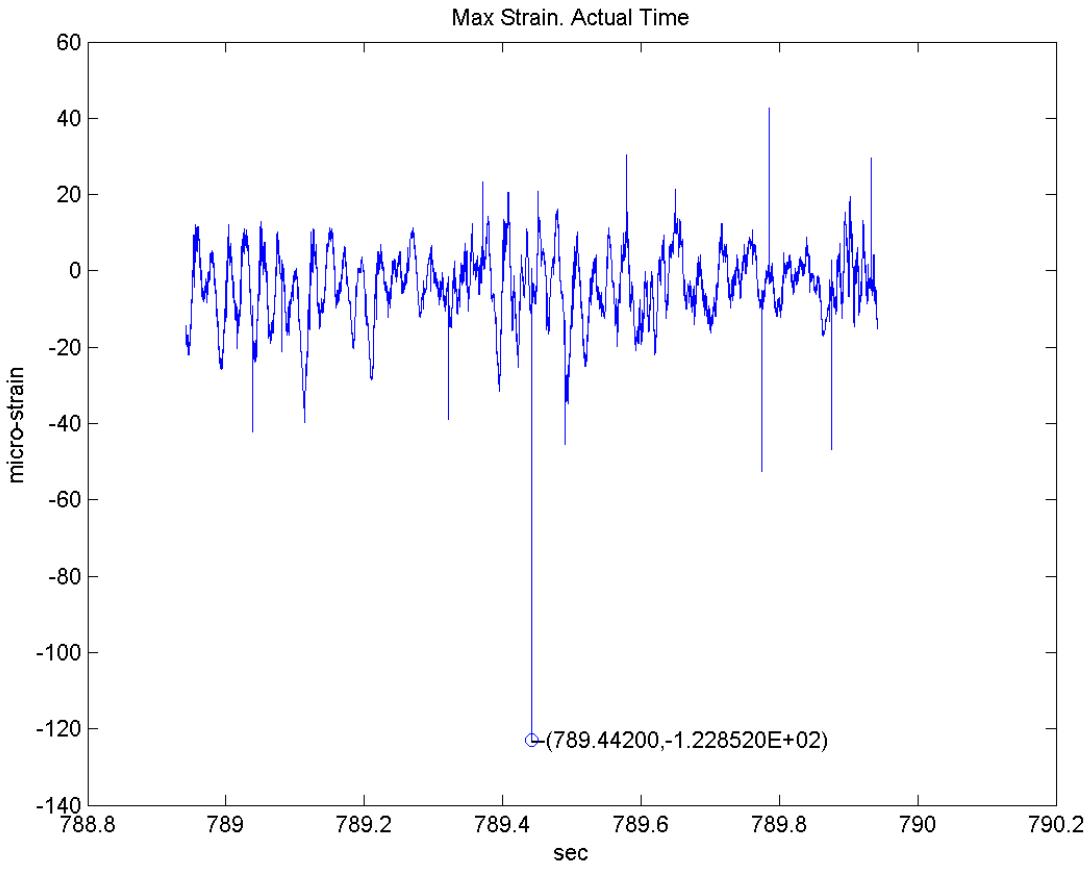


Figure 4-7: Peak strain data window (cladding location S1, 0 degrees).

## 4.2 Frequency Domain Loading Analysis

The ten-second window of acceleration centered on 187.5 seconds into the first segment of road test 1 and was used to evaluate the shock loads recorded by the accelerometers. The frequency response analysis method was used to characterize the response of SDOF spring mass damper systems to the ten-second acceleration excitation. Each SDOF system has a discrete natural frequency of 1 Hz, 2 Hz, 3 Hz, etc., and results illustrate how an arbitrary system with a given natural frequency would respond to the excitation. A common damping ratio of 3% was assumed. This type of analysis is commonly used to characterize shock loading and is useful in the analysis of dynamic systems.

LS-DYNA was used to model 99 discrete SDOF spring/mass/damper systems with frequencies between 1 and 99 Hz. When the base acceleration is applied, the resulting absolute peak magnitude (+ or -) is recorded to plot peak magnitude versus SDOF frequency, which is referred to here as the SRS. The SRS for the Ch. 13 101Z assembly accelerometer from the first segment of road test 1 is shown in Figure 4-8.

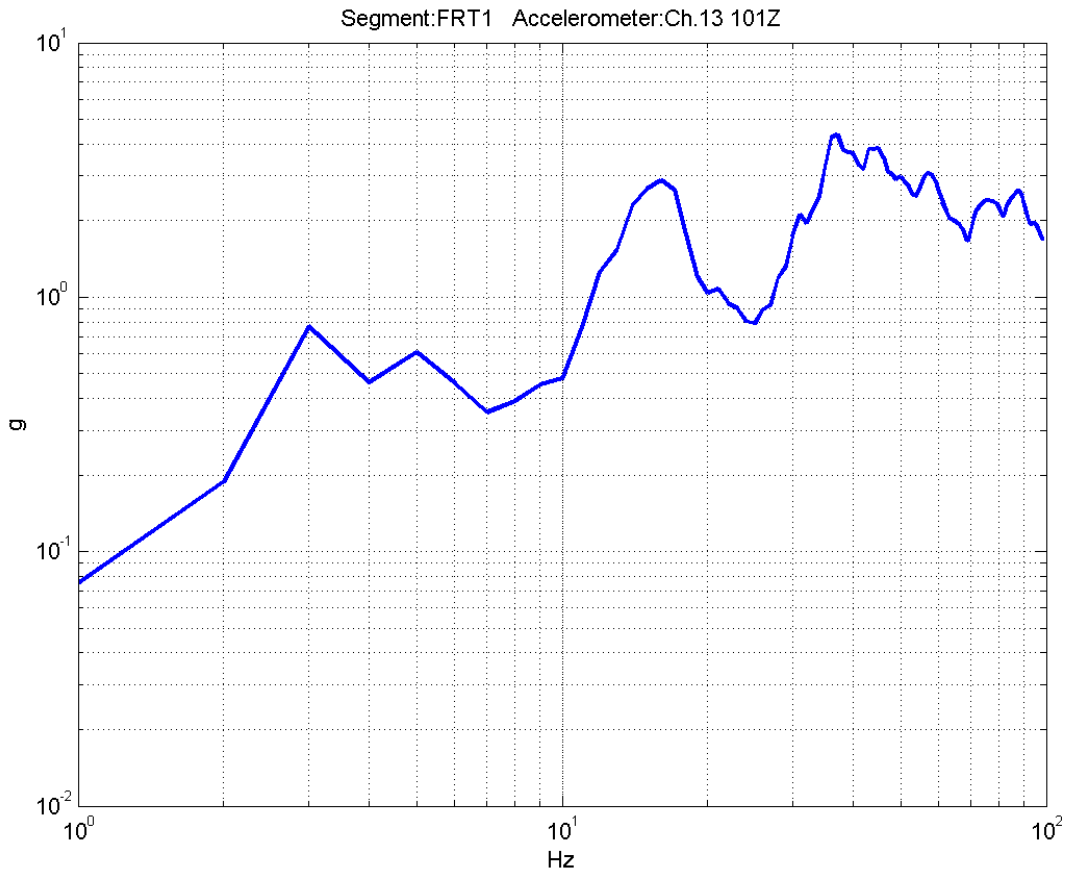


Figure 4-8: Shock response spectrum of ch. 13 101Z from segment 1 of road test 1.

This process was done for all assembly, basket, and truck accelerometers and plotted on a common plot. Two accelerometer channels appeared to contain bad data and thus were not included. Figure 4-9 shows the SRS for the assembly accelerometers for the first segment of road test 1, the basket accelerometers in the vertical direction for the same segment and test, and the truck accelerometers in the vertical direction for the same segment and test. Figure 4-10 illustrates the multi-degree of freedom system that the curves of Figure 4-9 correspond to. At the bottom are the truck and trailer accelerometers that define the excitation at the base level. The fuel basket witnesses the loads that are transferred up from the deck of the trailer through the concrete. Finally, the fuel assembly accelerometers are at the top, where basket loads are transmitted to the assembly and the assembly has some freedom to respond. At each step in the load transference, there is some attenuation or amplification of the dynamic loads.

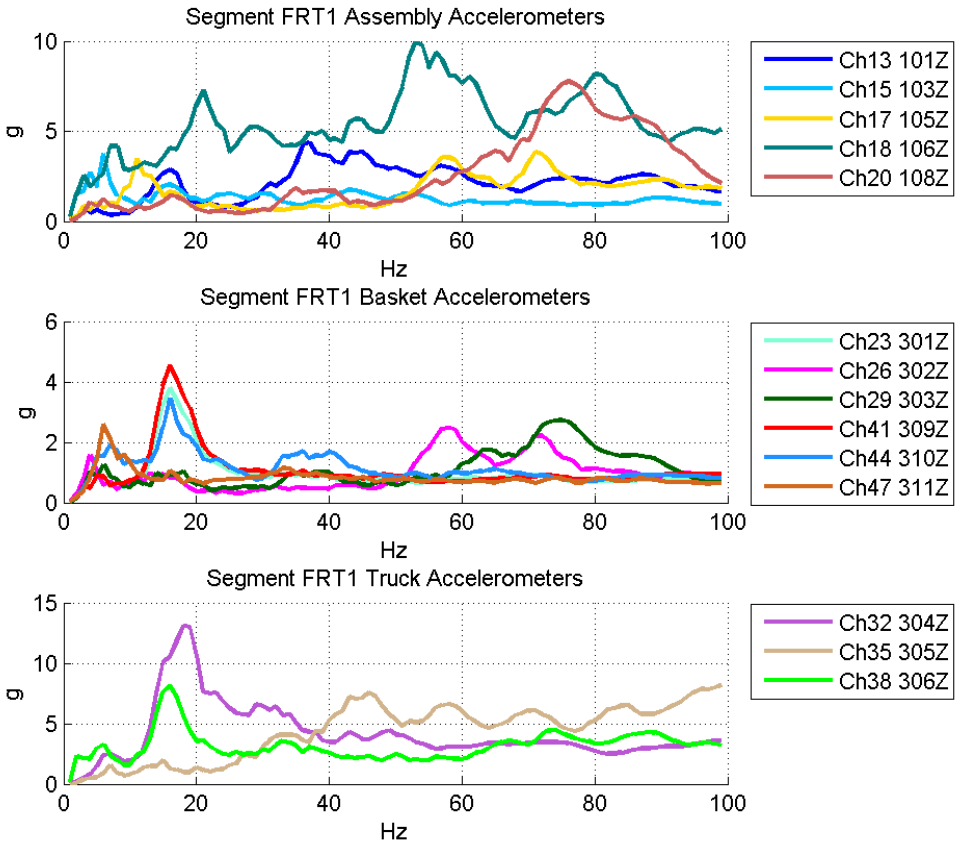


Figure 4-9: Shock response spectrums from segment 1 of road test 1.

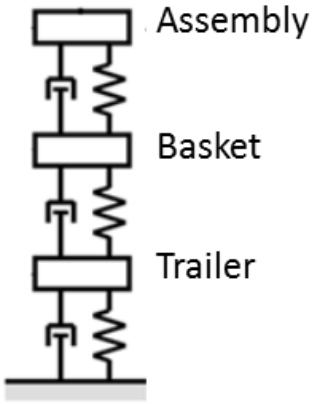


Figure 4-10: Multi-degree of freedom system illustrating the trailer, basket, and assembly system.

From Figure 4-9, it can be observed that there is a difference in magnitude between the trailer accelerometers and the basket accelerometers. To demonstrate this effect, the amplification ratio between the basket accelerometers and the trailer accelerometers has been generated. This was done by dividing the basket accelerometers SRS by a given truck accelerometer SRS. Figure 4-11 shows the amplification ratio between the basket accelerometers and the trailer drop deck

accelerometer; Figure 4-12 shows the amplification ratio between the basket accelerometers and the trailer rear axle accelerometer; and Figure 4-13 shows the amplification ratio between the basket accelerometers and the trailer king pin accelerometer.

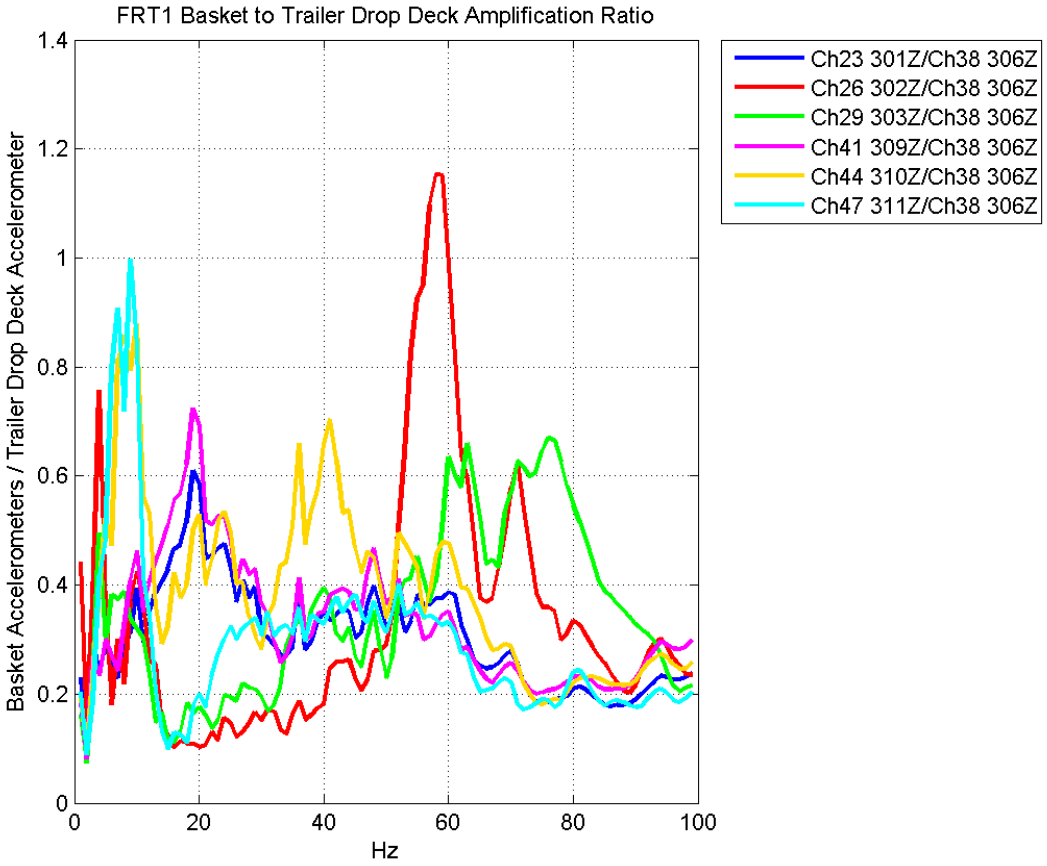


Figure 4-11: Basket to trailer drop deck amplification ratio from segment 1 of road test 1.

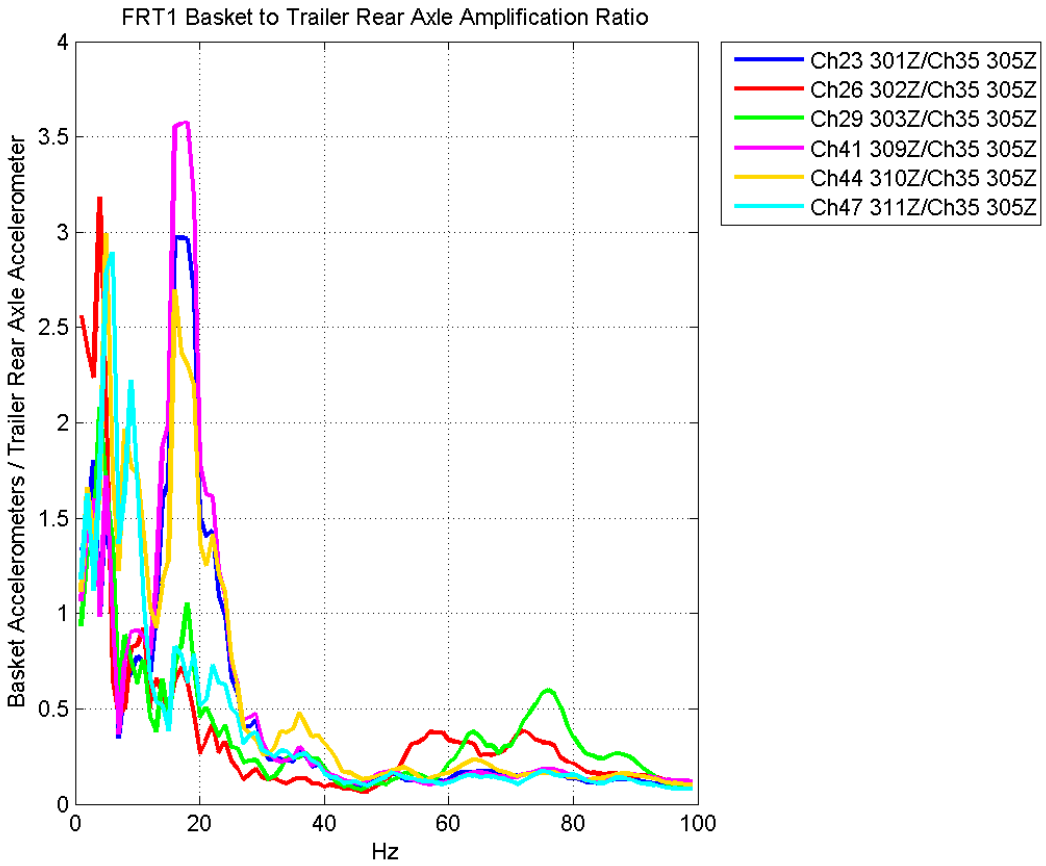


Figure 4-12: Basket to trailer rear axle amplification ratio from segment 1 of road test 1.

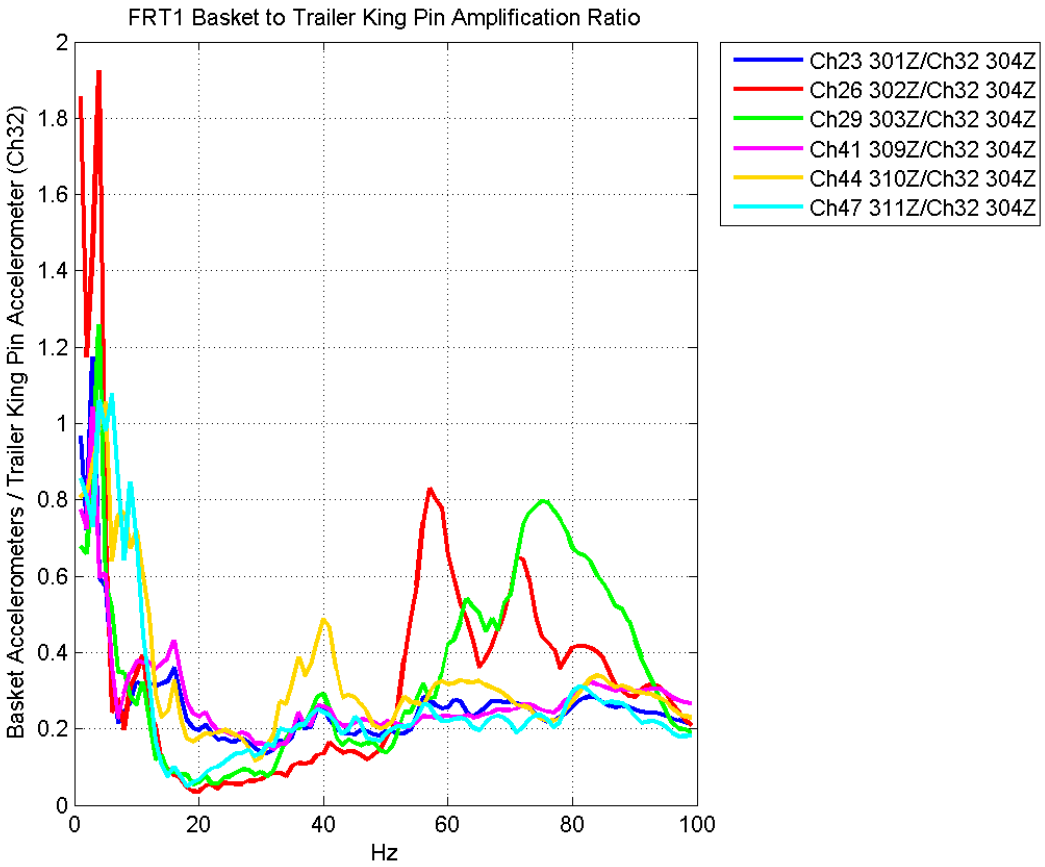


Figure 4-13: Basket to trailer king pin amplification ratio from segment 1 of road test 1.

This frequency domain analysis shows that the dynamic loads are not uniformly transmitted through the trailer/basket/fuel assembly dynamic system. This lack of transmission uniformity suggests that the configuration of the conveyance structure can affect the transmission of loads to the fuel assembly. In other words, two different conveyances traveling at the same speed over the same road could potentially cause different excitation to the fuel assemblies they carry, based on the design of the cask, cradle, and support structure. Note that in Figure 4-11 through Figure 4-13, there are frequencies where the basket response is amplified relative to the trailer response. This result demonstrates that amplification of dynamic loads is possible through the structure.

The SNL test data documents the response of one particular conveyance configuration that demonstrates acceptably low strains in the cladding. It would be valuable to characterize the structural dynamics of the SNL conveyance system for comparison to other conveyance designs. This comparison would give the recorded strains a context for interpretation. Such a numerical characterization could be done using the photographs taken during testing and any additional information collected at the time, such as mass or length measurements.

# 5. CONCLUSIONS

Updates were made to the PNNL detailed model of the SNL surrogate fuel assembly. The changes were found to have no significant effect on the calculated strains and did not improve agreement with the reported very low strains as had been hoped. This finding is suspected to be due to the relatively low magnitude of strains that are expected.

PNNL selected a one-second window of the SNL truck test data that was thought likely to provide a local maximum for cladding strains. An initial assessment of the acceleration loads suggested that the response would be of a lower magnitude than the shaker test data, and this was found to be the case. Peak strains calculated in the model were 323 μs while the test data for the corresponding strain gage reached 126 μs. This result is a closer agreement than in the shaker table case, but a time history comparison shows that the FEA model can be off by two orders of magnitude at any moment in the time history domain. PNNL's fuel assembly model can reasonably identify when strains will be low, but the precision needed to make a better estimate in the 100 μs range is expected to be to more difficult to attain than the effort would be worth.

Finally, PNNL performed some analyses on the accelerometer data and found that the dynamic load transference through the conveyance has a strong frequency-range dependency. This finding suggests that different conveyance configurations could behave differently and transmit different magnitudes of loads to the fuel even when traveling down the same road at the same speed. It is recommended that the SNL conveyance system used in testing be characterized through modal analysis and frequency response analysis to provide context to the low strains recorded.

# 6. REFERENCES

Adkins H, K Geelhood B Koeppel, J Coleman, J Bignell, G Flores, J-A Wang, S Sanborn, R Spears, and N Klymyshyn. 2013. *Used Nuclear Fuel Loading and Structural Performance Under Normal Conditions of Transport—Demonstration of Approach and Results on Used Fuel Performance Characterization*, (FCRD-UFD-2013-000325), Pacific Northwest National Laboratory, Richland, Washington.

Klymyshyn NA, S Sanborn, HE Adkins, and BD Hanson. 2013. *Fuel Assembly Shaker Test Simulation*, (FCRD-UFD-2013-000168, PNNL-22507), Pacific Northwest National Laboratory, Richland, Washington.

McConnell P, G Flores, R Wauneka, G Koenig, D Ammerman, J Bignell, S Saltzstein, and K Sorenson. 2013. *Fuel Assembly Shaker Test for Determining Loads on a PWR Assembly under Simulated Normal Conditions of Truck Transport, Rev. 0*, (FCRD-UFD-2013-000190, SAND2013-5210P), Albuquerque, California.